Supporting Information

Hematite nanoparticles decorated nitrogen-doped reduced graphene oxide/graphitic carbon nitride multifunctional heterostructure photocatalyst towards environmental applications

Shubhalaxmi Choudhury, Ugrabadi Sahoo, Samarjit Pattnayak, Sandip Padhiari, Manamohan Tripathy, and Garudadhwaj Hota*

Department of Chemistry, NIT Rourkela, Odisha, India, 769008.

***Corresponding Author**

Dr. Garudadhwaj Hota

Department of Chemistry, NIT Rourkela, Rourkela, Odisha, India, 769008

Email: garud@nitrkl.ac.in, garud31@yahoo.com

Ph: 91-661-2462655
Fax: 91-661-246265

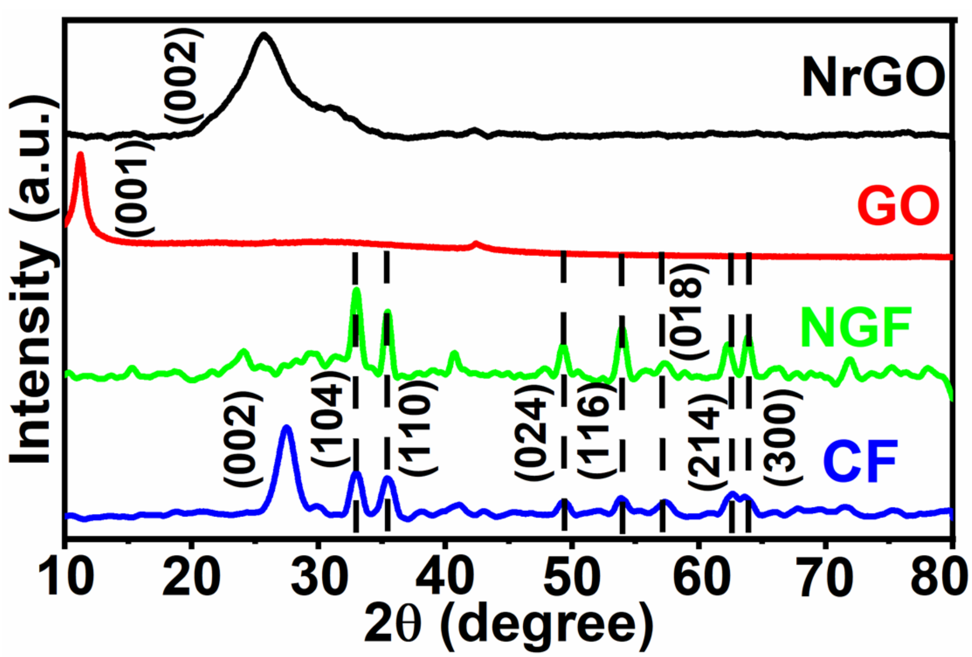

Figure S1. XRD spectra of GO, NrGO, NGF, and CF.

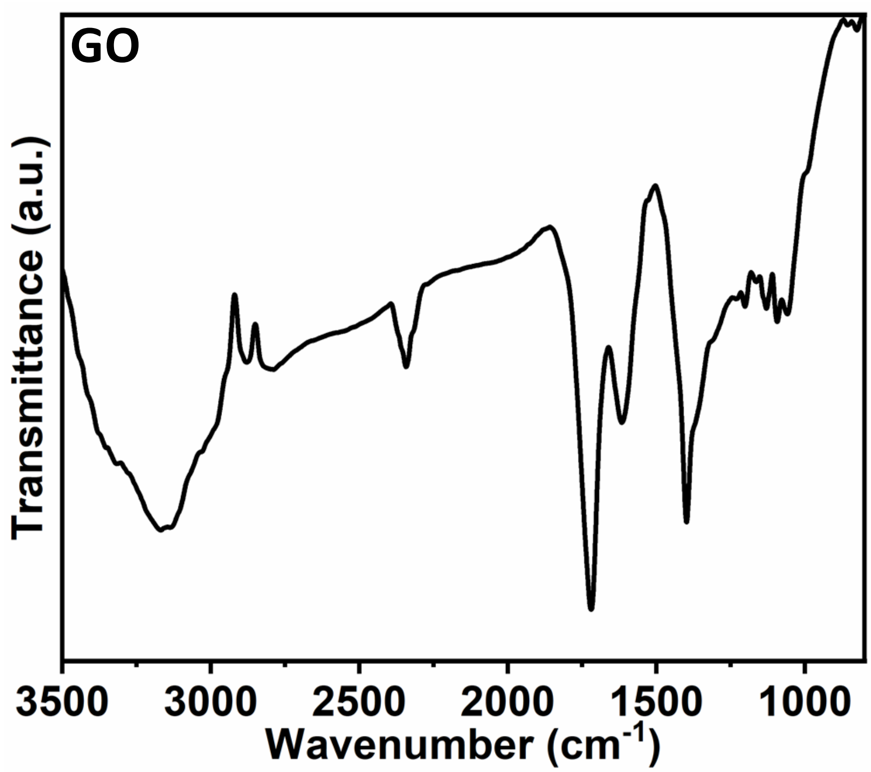

Figure S2. FTIR spectra of GO.

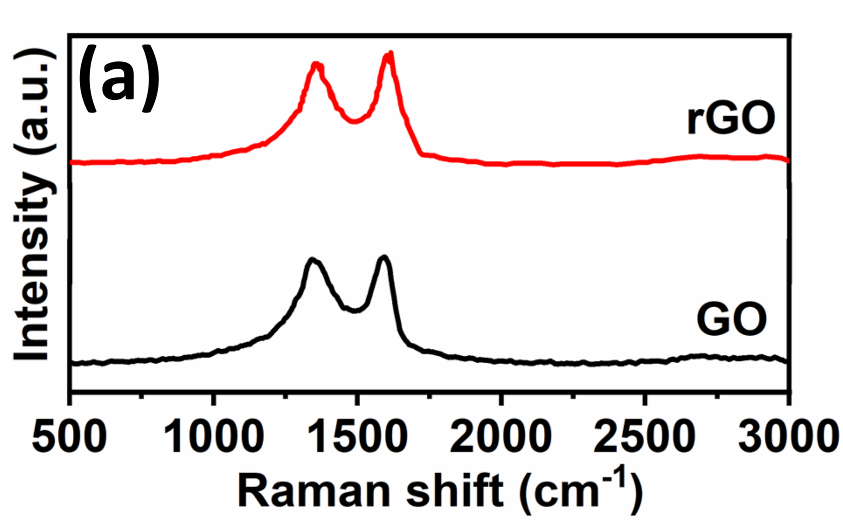

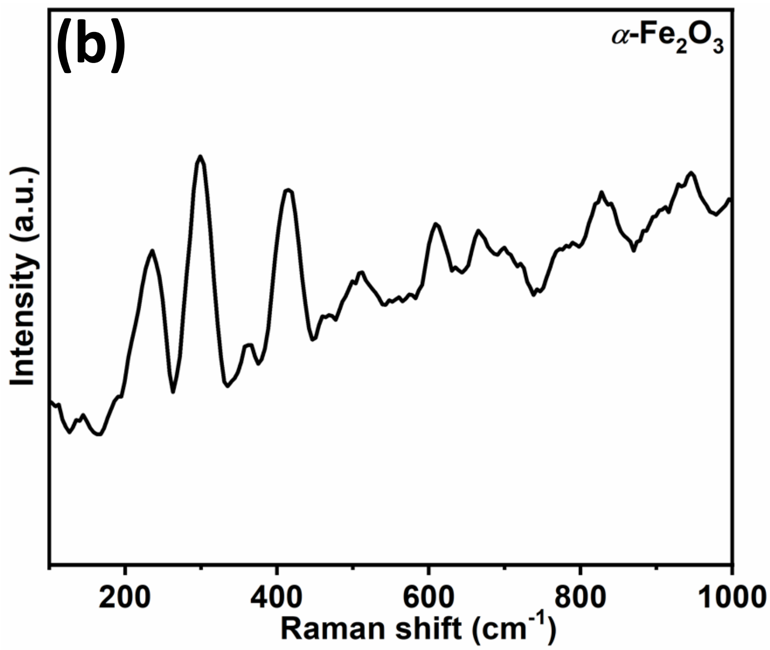

Figure S3. Raman spectra of (a) GO and rGO, (b) α-Fe_2O_3.

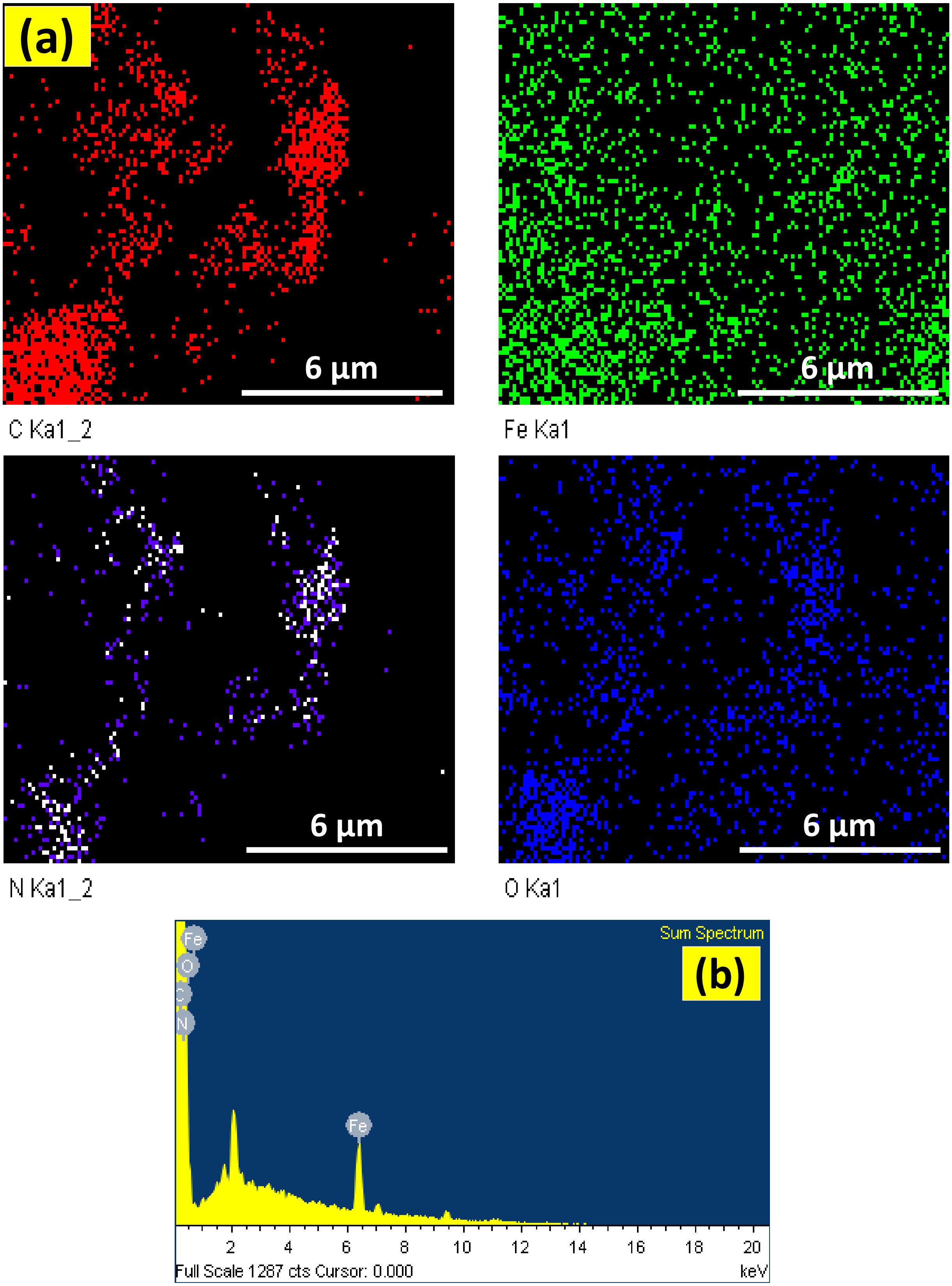

Figure S4. (a) SEM Elemental mapping of NGCF-10, (b) SEM-EDX spectra of NGCF-10

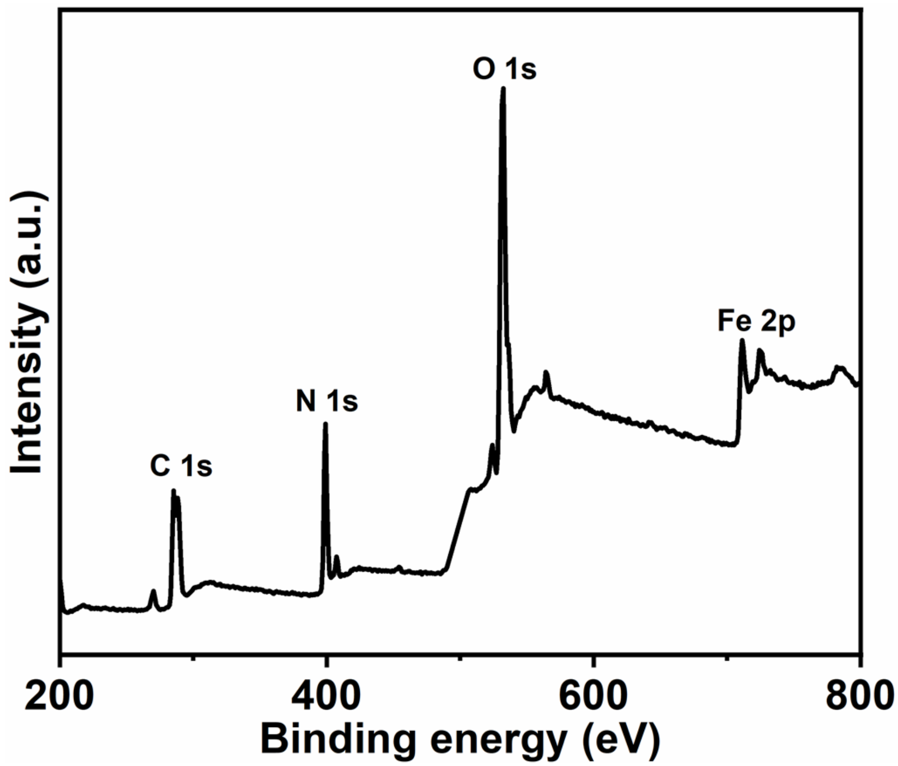

Figure S5. XPS survey spectra of NGCF-10.

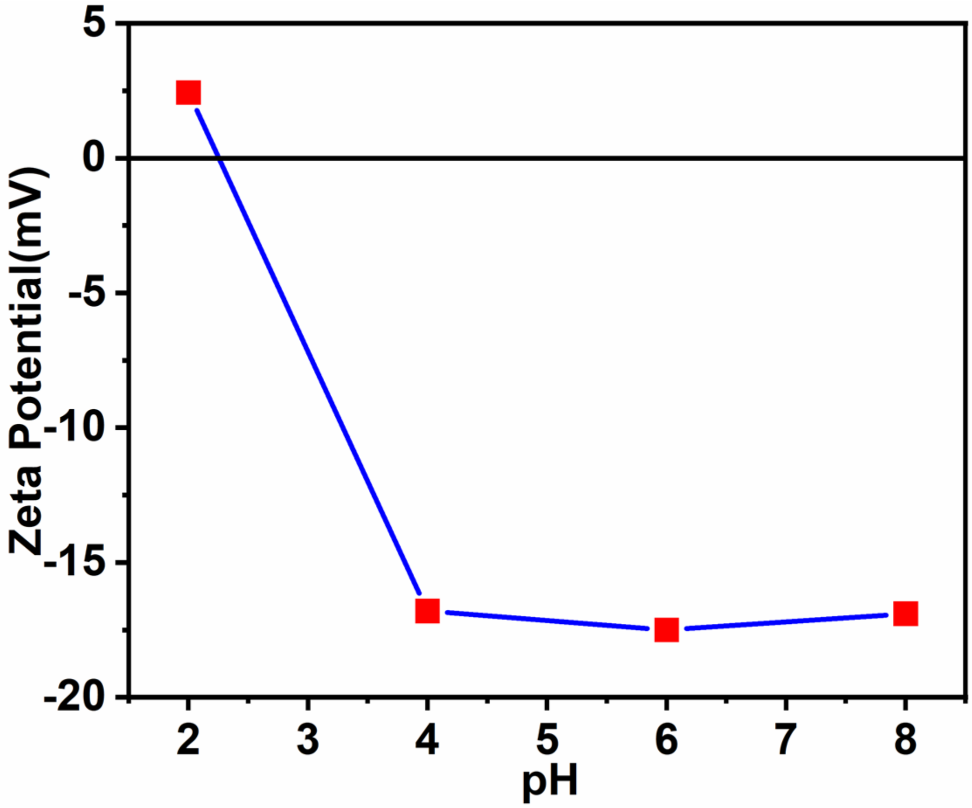

Figure S6. Zeta potential of NGCF-10.

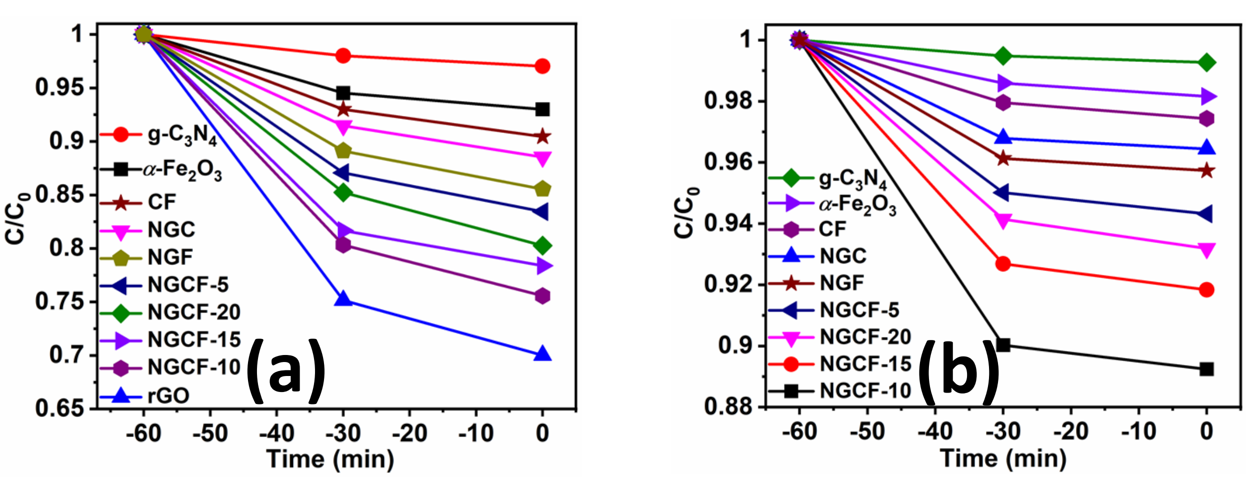

Figure S7. (a) photocatalytic reduction of Cr(VI), (b) photodegradation of DNP of as-synthesized nanomaterials under dark condition.

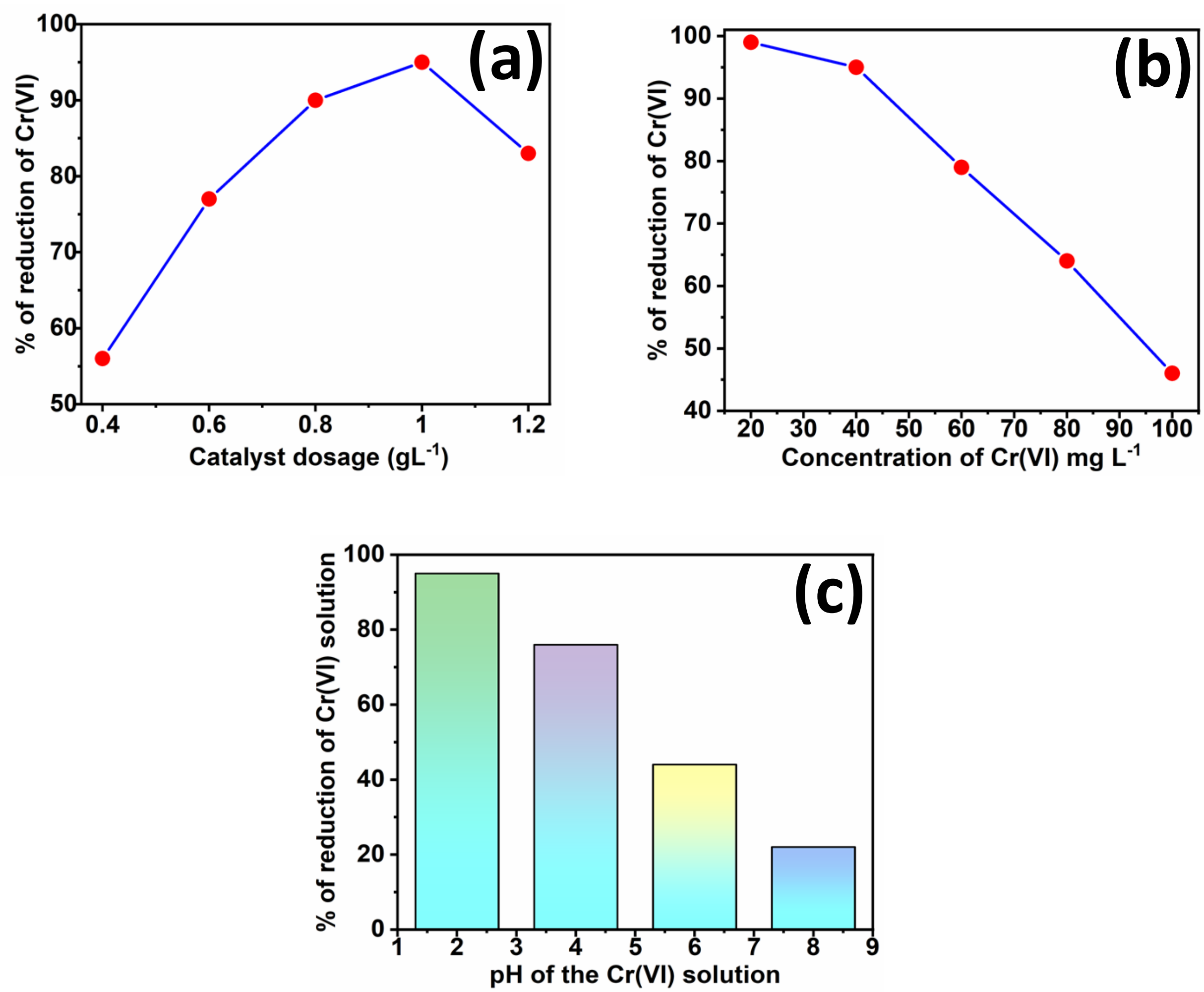

Figure S8. Effect of (a) catalyst dosages, (b) concentration of Cr(VI) solution, and (c) pH of the Cr(VI) solution on photocatalytic reduction of Cr(VI).

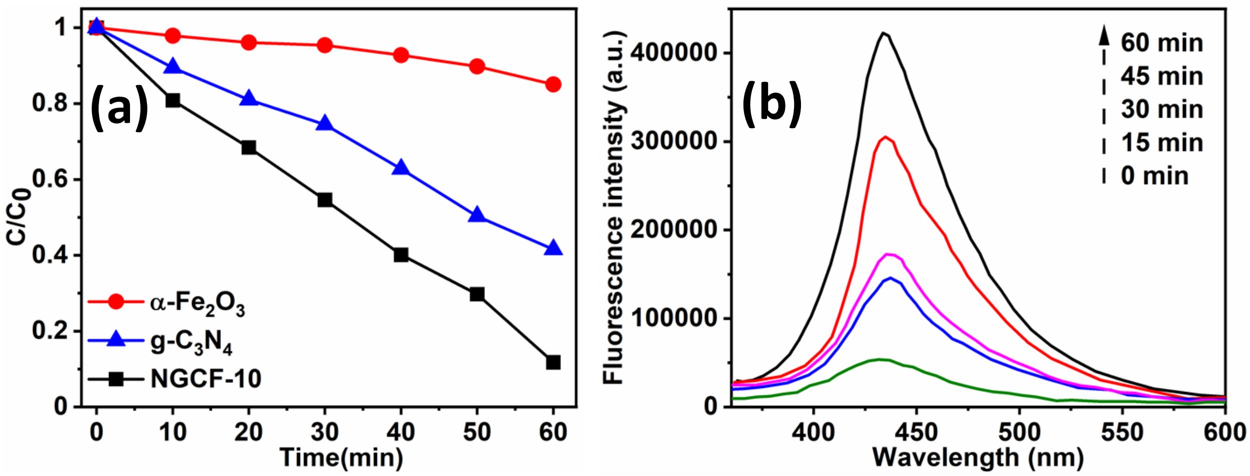

Figure S9. (a) Rate of reduction of NBT with time by g-C_3N_4, α-Fe_2O_3, and NGCF-10, (b) fluorescence spectra of 2-hydroxyterepthalic acid formed at different irradiation times in aqueous suspension of NGCF-10 photocatalyst.

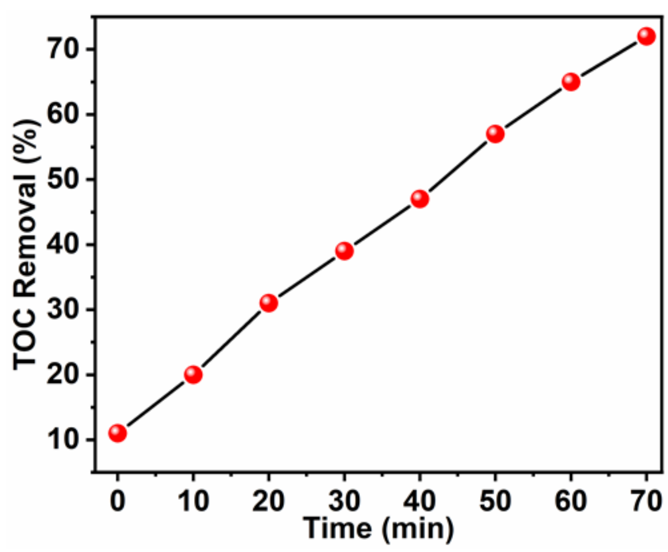

Figure S10. Percentage of removal of organic carbon at different irradiation time.

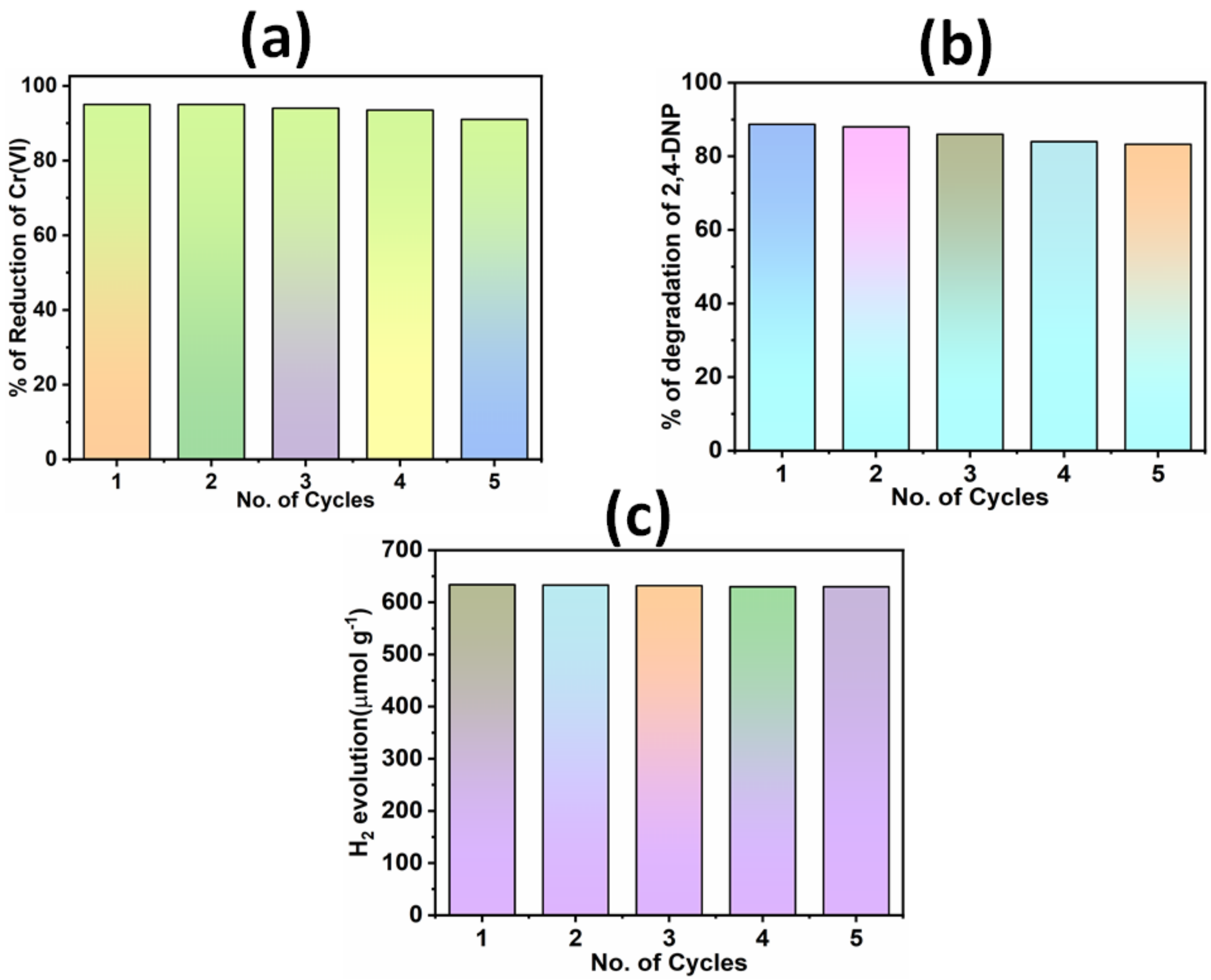

Figure S11. Recycle test of (a) photocatalytic reduction of Cr(VI), (b) photodegradation of 2,4-DNP, and (c) photocatalytic H_2 evolution reaction.

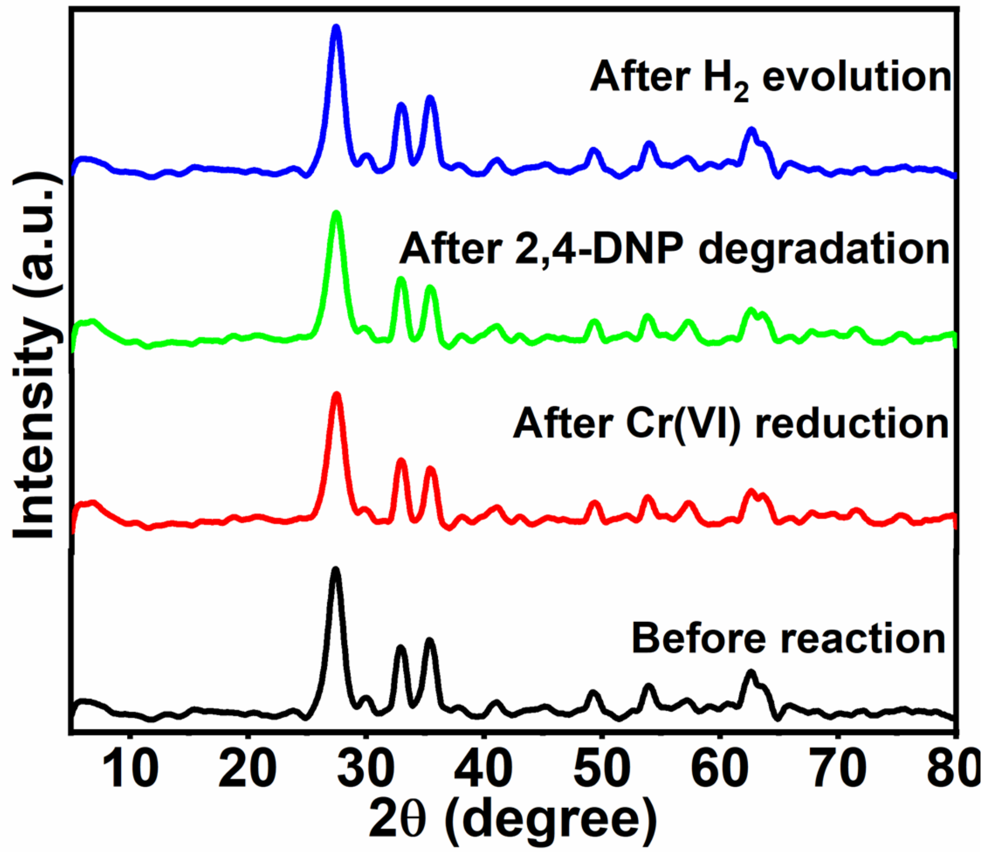

Figure S12. XRD spectra of the recovered samples after photocatalytic reduction of Cr(VI), photodegradation of 2,4-DNP, and H_2 evolution.

Table S1. SEM elemental composition of NGCF-10

Sample	C(Wt%)	N(Wt%)	O(Wt%)	Fe(Wt%)
NrGO/g-C_3N_4/α-Fe_2O_3-10	**33.23**	**53.57**	**9.34**	**3.87**

Table S2. BET surface area and pore volume of $g\text{-}C_3N_4$, $\alpha\text{-}Fe_2O_3$, rGO, and NGCF-10 respectively

Sample	BET surface area (m^2g^{-1})	Pore volume (cm^3g^{-1})
$g\text{-}C_3N_4$	**37.1**	**0.053**
$\alpha\text{-}Fe_2O_3$	**56**	**0.225**
rGO	**140.2**	**0.65**
NGCF-10	**127.7**	**0.244**

Table S3. State-of-the-Art for the Comparison of Cr(VI) reduction over NGCF nanocomposite with Other Reported Materials

Catalytic system	Concentration of Cr(VI) (ppm)	Catalytic activity time (min)	pH	Light source	Results (%)	Preparation method	Refs
Zn-MOF	20	90 min	2	Solar light	93	Solvothermal method	[1]
Ag@Ag3PO4/g-C3N4/NiFe LDH	20	120 min	5	Visible light	97	Electrostatic self-assembly and in situ photoreduction method	[2]
α-MnO2@RGO nanorod	10	120 min	2	Visible light	97	In situ hydrothermal	[3]
$NrGO/g\text{-}C_3N_4/\alpha\text{-}Fe_2O_3$	40	60 min	2	Visible light	95	Thermal treatment approach	**Present work**

Table S4. State-of-the-Art for the Comparison of 2,4-DNP degradation over NGCF nanocomposite with Other Reported Materials

Catalytic system	Concentration of DNP (ppm)	Catalytic activity time (min)	Light source	Results (%)	Preparation method	Refs
BiOBr/Ti3C2	10	60	UV-Visible light	45	Electrostatically driven self-assembly method	[4]
Y2O3-ZnO	10	100	Visible light	81.2	Precipitation method	[5]
g-C_3N_4/CNT/$BiVO_4$	10	120	Visible light	80.6	wet impregnation method	[6]
NrGO/g-C_3N_4/α-Fe_2O_3	10	70	Visible light	88.7	Thermal treatment approach	**Present work**

Table S5. State-of-the-Art for the Comparison of H_2 evolution NGCF nanocomposite with Other Reported Materials

Catalytic system	Sacrificial reagent	Cocatalyst	Light source	Results ($\mu molh^{-1}g^{-1}$)	Preparation method	Refs
Fe_2O_3/g-C_3N_4	Triethanolamine	Pt	Visible light	398	Electrostatic self-assembly approach	[7]
GO/g-C_3N_4	Triethanolamine	Pt	Visible light	224.6	Ultrasonic-microwave assisted method	[8]
carbon spheres/g-C_3N_4	Triethanolamine	Pt	Visible light	50.2	Thermal polymerization	[9]
NrGO/g-C_3N_4/α-Fe_2O_3	Triethanolamine	Pt	Visible light	633.92	Thermal treatment approach	**Present work**

Calculation of apparent conversion efficiency: The apparent conversion efficiency was calculated using the method described by Subudhi et al.[10]

$$Apparent\ Conversion\ efficiency\ (\%) = \frac{Stored\ Chemical\ Energy\ (SCE)}{energy\ of\ incident\ light\ (EIL)} X\ 100$$

$$SCE = \frac{N(H_2)}{t}\Delta H_C = Moles\ of\ H_2\ produced\ per\ second\ \times\ \Delta H_C \quad = 633.9 = 0.05032\ J/sec$$

$N(H_2) = Moles\ of\ H_2\ produced\ during\ the\ reaction$

$t\ =\ Duration\ of\ the\ reaction\ (sec)$

$\Delta H_C = Combustion\ heat\ of\ H_2\ (kJ/mol)$

$$EIL = \frac{Q_i}{4\pi r^2} = \frac{250\ W}{4\ \times 3.141\ \times (4)^2} = 1.2436\ W/cm^2$$

$Q_i = 250\ W,\ r = 4\ cm\ (distance\ between\ reactor\ surface\ and\ lamp)$

$$Apparent\ Conversion\ efficiency\ (\%) = \frac{0.05032\ J/sec}{1.2436\ W/cm^2} X\ 100 \quad = 4.046\ \%$$

REFERENCES

(1) Kaur, H.; Sinha, S.; Krishnan, V.; Koner, R. R. Photocatalytic Reduction and Recognition of Cr(VI): New Zn(II)-Based Metal-Organic Framework as Catalytic Surface. *Ind. Eng. Chem. Res.* **2020**, *59* (18), 8538–8550. https://doi.org/10.1021/acs.iecr.9b06417.

(2) Nayak, S.; Parida, K. M. Dynamics of Charge-Transfer Behavior in a Plasmon-Induced Quasi-Type-II p-n/n-n Dual Heterojunction in Ag@Ag3PO4/g-C3N4/NiFe LDH Nanocomposites for Photocatalytic Cr(VI) Reduction and Phenol Oxidation. *ACS Omega* **2018**, *3* (7), 7324–7343. https://doi.org/10.1021/acsomega.8b00847.

(3) Padhi, D. kumar; Baral, A.; Parida, K.; Singh, S. K.; Ghosh, M. K. Visible Light Active Single-Crystal Nanorod/Needle-like α-MnO 2 @RGO Nanocomposites for Efficient Photoreduction of Cr(VI) . *J. Phys. Chem. C* **2017**, *121* (11), 6039–6049. https://doi.org/10.1021/acs.jpcc.6b10663.

(4) Huang, Q.; Liu, Y.; Cai, T.; Xia, X. Simultaneous Removal of Heavy Metal Ions and Organic Pollutant by BiOBr/Ti 3 C 2 Nanocomposite. *J. Photochem. Photobiol. A Chem.* **2019**, *375* (December 2018), 201–208. https://doi.org/10.1016/j.jphotochem.2019.02.026.

(5) Su, T. M.; Qin, Z. Z.; Ji, H. B.; Jiang, Y. X. Preparation, Characterization, and Activity of Y2O 3-ZnO Complex Oxides for the Photodegradation of 2,4-Dinitrophenol. *Int. J. Photoenergy* **2014**, *2014*. https://doi.org/10.1155/2014/794057.

(6) Samsudin, M. F. R.; Bacho, N.; Sufian, S.; Ng, Y. H. Photocatalytic Degradation of Phenol Wastewater over Z-Scheme g-C 3 N 4 /CNT/BiVO 4 Heterostructure Photocatalyst under Solar Light Irradiation. *J. Mol. Liq.* **2019**, *277*, 977–988. https://doi.org/10.1016/j.molliq.2018.10.160.

(7) Xu, Q.; Zhu, B.; Jiang, C.; Cheng, B.; Yu, J. Constructing 2D/2D Fe2O3/g-C3N4 Direct Z-Scheme Photocatalysts with Enhanced H2 Generation Performance. *Sol. RRL* **2018**, *2* (3), 1–10. https://doi.org/10.1002/solr.201800006.

(8) Li, J.; Tang, Y.; Jin, R.; Meng, Q.; Chen, Y.; Long, X.; Wang, L.; Guo, H.; Zhang, S. Ultrasonic-Microwave Assisted Synthesis of GO/g-C3N4 Composites for Efficient Photocatalytic H2 Evolution. *Solid State Sci.* **2019**, *97* (September), 1–8. https://doi.org/10.1016/j.solidstatesciences.2019.105990.

(9) Li, K.; Xie, X.; Zhang, W. De. Photocatalysts Based on G-C3N4-Encapsulating Carbon Spheres with High Visible Light Activity for Photocatalytic Hydrogen Evolution. *Carbon N. Y.* **2016**, *110*, 356–366. https://doi.org/10.1016/j.carbon.2016.09.039.

(10) Subudhi, S.; Mansingh, S.; Swain, G.; Behera, A.; Rath, D.; Parida, K. HPW-Anchored UiO-66 Metal-Organic Framework: A Promising Photocatalyst Effective toward Tetracycline Hydrochloride Degradation and H 2 Evolution via Z-Scheme Charge Dynamics. *Inorg. Chem.* **2019**, *58* (8), 4921–4934. https://doi.org/10.1021/acs.inorgchem.8b03544.